Journal of Alloys and Compounds 506 (2010) 327–330

Contents lists available at ScienceDirect

Journal of Alloys and Compounds

journal homepage: www.elsevier.com/locate/jallcom

Study on Raman spectra of zinc selenide nanopowders synthesized by hydrothermal method

Huiling Li [a,b], Biben Wang [b,*], Lijun Li [b]

[a] Department of Chemistry, Henan Institute of Education, Zhengzhou 450046, PR China
[b] College of Optoelectronic Information, Chongqing University of Technology, 69 Hongguang Road, Lijiatuo, Banan District, Chongqing 400054, PR China

ARTICLE INFO

Article history:
Received 21 February 2010
Received in revised form 27 June 2010
Accepted 30 June 2010
Available online 13 July 2010

Keywords:
Zinc selenide powder
Hydrothermal method
Raman spectroscopy

ABSTRACT

Zinc selenide nanopowders with different structures were synthesized from sodium hydroxide solution by hydrothermal method at different temperatures with zinc and selenium powders as the precursors. The powders composed of different nanostructures were investigated by X-ray diffraction, transmission electron microscopy and micro-Raman spectroscopy. The results indicate that the products have zincblende structure and become inhomogeneous with increasing temperature. The peaks in the Raman spectra relate to zinc selenide and impurity. In addition, the Raman spectra show that the shapes of the Raman peaks depend on the structure and size of the zinc selenide particles in powders. It also shows that the Raman scattering is greatly enhanced when the size of the zinc selenide particles is about 10 nm, which relates to the resonance scattering.

1. Introduction

In recent years, nanostructured zinc selenide (ZnSe) as a direct wide-band gap II–VI group semiconductor material has gained considerable attention because it has a band gap energy of 2.8–2.99 eV at room temperature [1,2] and unique properties depending on different structures [3–6]. For example, the hollow ZnSe microspheres constructed from ZnSe nanoparticles with zincblende structure via Ostwald ripening show a strong near-band emission at 479 nm [3], but the ZnSe nanowires synthesized by thermal vaporation method displays a strong emission at 629 nm [4] and the ZnSe–Ag_2Se nanocomposites via the high-temperature reflux route display a strong green emission at 550 nm due to Ag doping in the ZnSe nanoparticles [5]. In addition, the ZnSe nanowires coated with TiO_2 by sputtering can significantly enhance the photoluminescence intensity in which the emission band is at about 630 nm due to increases in the concentrations of deep levels [6]. The above properties of different ZnSe nanostructures indicate that they will have a broad range of potential applications for electroluminescent devices, field effect transistors, sensors, light-emitting, and solar cells [7,8]. For their applications, it is necessary to understand their structure variation and Raman spectroscopy is extensively used to characterize them [1–3,7,9]. The characterization of ZnSe nanostructures from Raman spectroscopy shows two main peaks centered at about 205 and 253 cm^{-1} which are attributed to the transverse optic (TO) and longitudinal optic (LO) phonon modes of ZnSe [1–3], respectively. However, the change of the Raman peaks on the nanostructured ZnSe still remains completely unclear.

In this work, the ZnSe powders constructed from different nanoparticles were synthesized and investigated by micro-Raman spectroscopy. The Raman spectra present peaks relating to impurity and interface phonon besides the two common peaks centered around 206 and 252 cm^{-1}. In addition, the peak located at about 206 cm^{-1} is very broad and it is difficult to resolve when the size of the ZnSe nanoparticles is small enough, but the intensity of the peak around 252 cm^{-1} is enhanced which is possible to result from the resonance scattering. The results suggest that the optical properties of powder materials are influenced by the size of the particles and the aggregation of the small particles in powders. Therefore, we believe that our results are significant to control the synthesis of the nanostructured semiconductor materials for their optical properties and applications in the field of photoelectronic devices.

2. Experimental details

The ZnSe nanopowders were prepared from sodium hydroxide solution by hydrothermal method at different temperatures [10]. The 0.8 g of zinc powder (90%), 1.09 g of selenium power (99.95%) and 6.4 g of sodium hydroxide powder (96%) were mixed in about 40 ml of deionized water in a Teflon-lined autoclave of 50 ml capacity. After the autoclave was sealed into a stainless steel tank, it was heated at a heating rate of 5 °C/min in an oven for 4 h at 100, 140 and 160 °C, respectively. After the autoclave was naturally cooled to room temperature, the products were collected by pumping-filter equipment and they were washed by deionized water. Finally, the products of light yellow powders were dried at 60 °C for 6 h.

The components of the collected powders were characterized by a Bruker D-8 Advance X-ray diffractionmeter (XRD) using Cu Kα radiation. The morphologies of

* Corresponding author. Tel.: +86 23 6256 3051; fax: +86 23 6256 3058.
E-mail address: bibenw@yahoo.com (B. Wang).

0925-8388/$ – see front matter © 2010 Elsevier B.V. All rights reserved.
doi:10.1016/j.jallcom.2010.06.201

the ZnSe nanoparticles were studied by a Philips Tecnai-12 transmission electron microscopy (TEM). The Raman spectra were recorded by a HR-800 micro-Raman spectroscopy in which a YAG laser at 532 nm was used as the excitation source and its output power is set to 0.1 mW.

3. Results

Fig. 1(a)–(c) show the XRD patterns of ZnSe nanopowders prepared at 100, 140, and 160 °C, respectively. The peaks at about 27.3°, 45.2°, 53.6° and 65.9° are from the diffraction of ZnSe with zincblende structure (JCPDS card, No. 37-1463) and other peaks at about 36.3°, 39.1° and 43.2° are related to the diffraction from zinc which indicate that there is excessive zinc in the synthesis process of ZnSe powders (JCPDS card, No. 04-0831).

Fig. 2(a)–(c) are the TEM images of the ZnSe nanopowders synthesized at 100, 140, and 160 °C, respectively. Fig. 2(a) shows that the ZnSe grains synthesized at 100 °C are homogeneous and their size is about 10 nm. However, Fig. 2(b) and (c) show that the ZnSe grains synthesized at 140 and 160 °C are inhomogeneous and their size ranges from 25 to 60 nm and 20 to 73 nm, respectively. Therefore, the ZnSe grains become inhomogeneous with increased

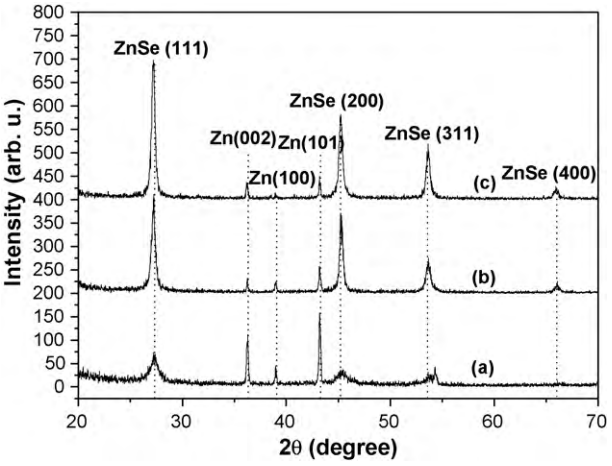

Fig. 1. XRD patterns of the ZnSe nanopowders prepared at different temperatures: (a) 100 °C, (b) 140 °C, and (c) 160 °C.

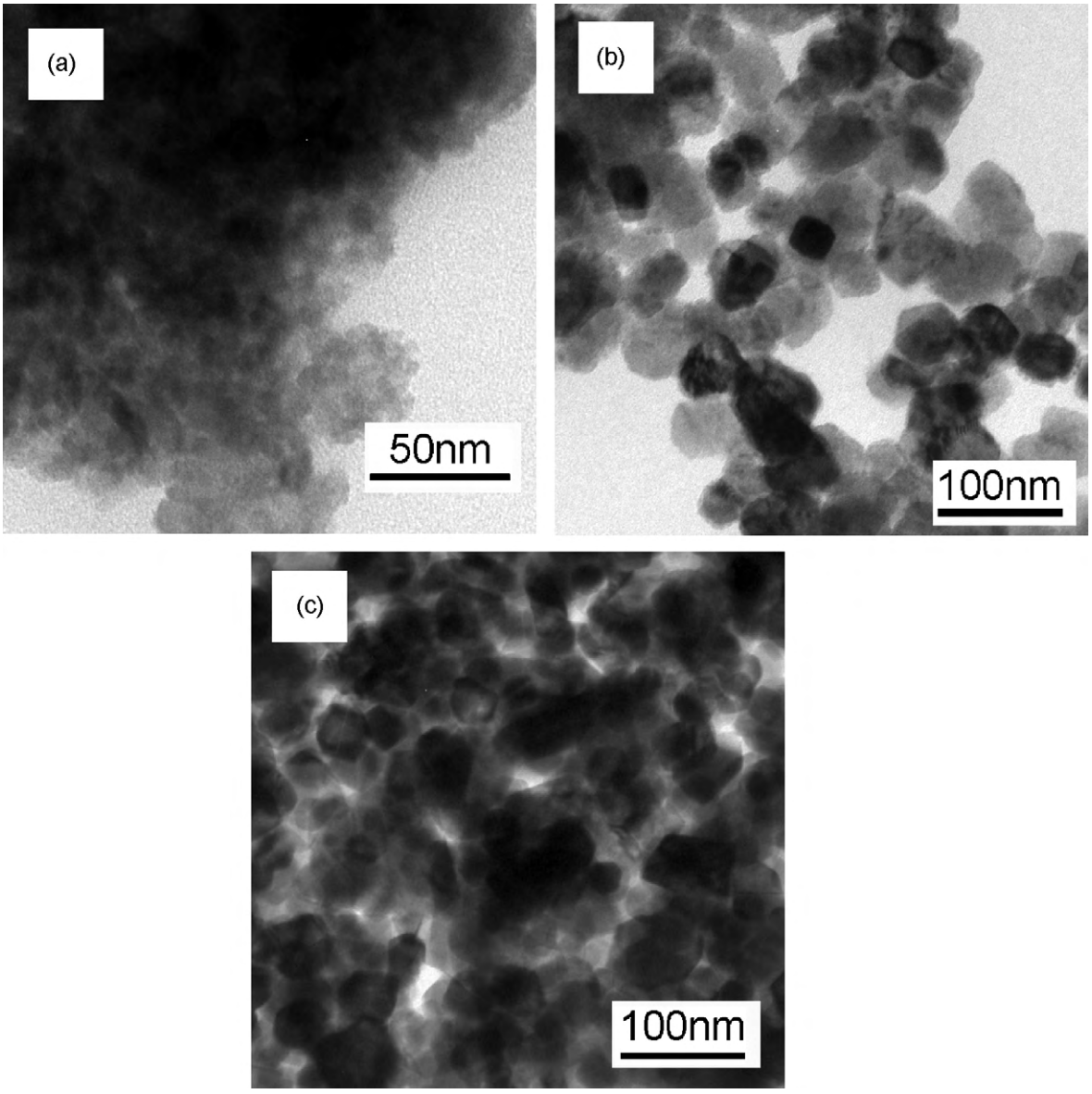

Fig. 2. TEM images of the ZnSe nanopowders prepared at different temperatures: (a) 100 °C, (b)140 °C, and (c) 160 °C.

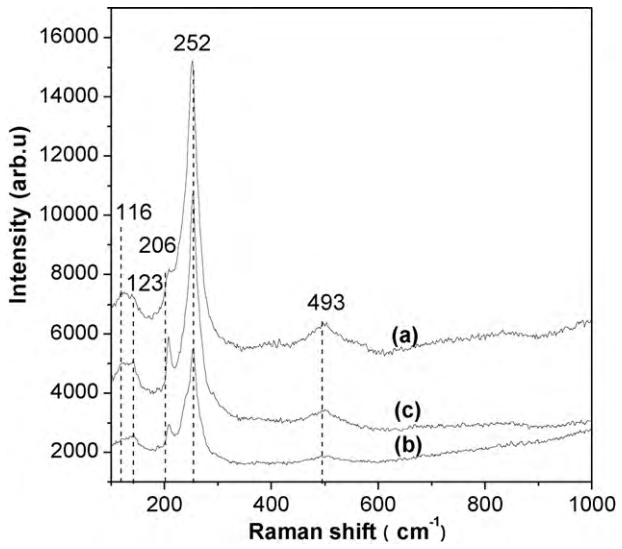

Fig. 3. Raman spectra of the ZnSe nanopowders prepared at different temperatures: (a) 100 °C, (b) 140 °C, and (c) 160 °C.

temperature. In addition, Fig. 2(a) also shows aggregation of the ZnSe nanoparticles, which is due to high surface energy of the particles with small size.

Fig. 3(a)–(c) are the Raman spectra of the ZnSe powder prepared at 100, 140, and 160 °C, respectively. As shown in Fig. 3, there are five peaks in every spectrum which are centered about 116, 123, 206, 252 and 493 cm^{-1}. The peaks located at about 206, 252 and 493 cm^{-1} are attributed to the TO, LO and 2LO phonon modes of ZnSe [1–3,11], the peaks at about 116 cm^{-1} is related to selenium [12] and the peak located at about 123 cm^{-1} possibly results from the interfaces [13].

4. Discussion

The above results indicate that the growth of the ZnSe nanoparticles from solution is inhomogeneous and the inhomogeneous growth mechanism was studied in our previous work [10]. Here the Raman spectra of the ZnSe nanopowders were analyzed emphatically.

4.1. Analysis of the impure peak

In the Raman spectra, there is the weak signal related to selenium, which we call the impure peak. The selenium is due to the uncompleted reaction of zinc with selenium. However, the amount of selenium might be too less to be detected by XRD, thus there is no diffraction from selenium in Fig. 1. The Raman spectroscopy is sensitive to the unpolarizable materials, therefore the peak related to selenium can appear in the Raman spectra.

4.2. Confirmation of the peak located at 123 cm^{-1}

In Fig. 3, there is a peak located at about 123 cm^{-1}, which is related to the interface between the ZnSe and Zn particles. As shown in Fig. 1, there exists residual zinc in every reaction process, thus the interface between the ZnSe and Zn particles can be formed because ZnSe nucleates on the surface of a zinc particle in sodium hydroxide solution [10]. Zhang et al. studied the Raman scattering on CdSe/ZnTe superlattice to find an interface vibration mode between the CdSe and ZnTe layers, which is attributed to the stretching of a localized Zn–Se bond in the interface [13]. In Ref. [13], the Raman spectrum at 293 K shows a Raman peak located at about 121 cm^{-1} which is caused by the interface phonon. Thus, the peak centered at about 123 cm^{-1} in Fig. 3 is attributed to the interface phonon mode between the ZnSe and Zn particles. Although the interface phonon modes usually occur at the interface in AB/CD type superlattices [13], the interface phonon mode of ZnSe was observed in our powder samples, which is possible from the effect of the aggregation of zinc particles in the interfaces among the ZnSe particles.

4.3. Explanation of the Raman scattering enhancement and the change of the peaks depending on the particle size of ZnSe

From Fig. 3, it is obvious that the peak at about 206 cm^{-1} in (a) is broader than that in (b) and (c) and it is difficult to resolve, however the peak at about 252 cm^{-1} in (a) is the strongest in the peaks at about 252 cm^{-1} of Fig. 3, which the similar results were observed in ZnSe film by Nesheva et al. [14]. We think they are related to the structures and size of the ZnSe particles.

Fig. 1 shows that the ZnSe powders are mainly composed of (1 1 1) ZnSe and (1 0 0) ZnSe and the intensity of the peak from the diffraction of (1 1 1) ZnSe in (a) is much lower than that in (b) and (c), which indicate that the content of the (1 1 1) ZnSe grains in the powder grown at 100 °C is much lower than that in the powder grown at 140 and 160 °C. According to the symmetry selection rules for backscattering from zincblende type semiconductors, the TO mode is forbidden in backscattering configuration on (1 0 0) face and the LO mode is allowed on (1 0 0) face, and both the TO and LO modes are allowed in backscattering configuration on (1 1 1) face [15]. In addition, the scattering intensity increases with enhancement of the scattering volume [16]. Thus, the intensity of the TO band in Fig. 3(a) should be much lower than that in Fig. 3(b) and (c). It is possible that the intensity of the TO band is enhanced due to the Frölich interaction (see following analysis), but it is broadened by the reduction of ZnSe particle size so that it is difficult to resolve.

From Fig. 3, it is obvious that the intensity of the peak centered at bout 252 cm^{-1} in Fig. 3(a) is stronger than that in Fig. 3(b) and (c). The peak in Fig. 3(a) should be the weakest because the ZnSe particles are smallest, but it is the strongest, which is possible to result from the resonant behavior. The phenomenon was observed by Nesheva et al. [14] when they used the 442 nm (2.8 eV) line of the He–Cd laser as the excitation source to measure Raman spectra of ZnSe thin films with different thicknesses (30–100 nm). They found that the scattering peak on the 30 nm ZnSe is the strongest and believed that it resulted from the resonant behavior because the band gap energy of ZnSe particles approached the exciting energy. In our experiment, the samples were excited by 532 nm (2.22 eV) line, in which the exciting energy does not approach the optical band gap of 10 nm ZnSe particles (~2.8 eV [14]). So, it is impossible to produce the resonance enhancement in Raman spectroscopy by this resonance mechanism. But, the Frölich interaction can lead to strong resonance of the LO mode in confined semiconductors [17]. Because ZnSe is polar semiconductor, the dipoles generate in it when it is irradiated by laser. As a result, an electric field is produced. The field interacts with electrons, i.e., the Frölich interaction occurs. For the powder synthesized at 100 °C, the aggregation of the ZnSe particles results in the dipolar interaction [16] to improve the Frölich interaction, thus the resonance scattering can occur and the scattering peak is the strongest. For the powders synthesized at 140 and 160 °C, the ZnSe particles become large and Fig. 2 shows that their aggregation is weakened so that the Frölich interaction becomes weak. As a result, the resonance scattering cannot occur. But, there are more large particles in the powder synthesized at 160 °C than the powder synthesized at 140 °C so that the peak in Fig. 3(c) is stronger than that Fig. 3(b).

5. Conclusions

In summary, ZnSe nanopowders with different structures were prepared by hydrothermal method at different temperatures and they were investigated by XRD, TEM and micro-Raman spectroscopy. It is found that the Raman peaks is related to selenium and interface phonon besides two common peaks of ZnSe centered at about 206 and 252 cm^{-1} and the intensities of the common peaks depend on the size, structure and aggregation of the ZnSe particles. It is important to find that the resonance scattering occurs when the ZnSe particles are about 10 nm. The analyses of the experimental results indicate that these phenomena are due to the uncompleted reaction and the Frölich interaction.

References

[1] S.V. Pol, V.G. Pol, A. Gedanken, J. Phys. Chem. C111 (2007) 13309–13314.
[2] M. Shakir, S.K. Kushwaha, K.K. Maurya, G. Bhagavannarayana, M.A. Wahab, Solid State Commun. 149 (2009) 2047–2049.
[3] L.H. Zhang, H.Q. Yang, X.L. Xie, F.H. Zhang, L. Li, J. Alloys Compd. 473 (2009) 65–70.
[4] Y.X. Du, Q.X. Yuan, J. Alloys Compd. 492 (2010) 548–551.
[5] X. Han, J. Sun, H.L. Wang, X.W. Du, J. Yang, J. Alloys Compd. 492 (2010) 638–641.
[6] C. Lee, C. Jin, H. Jim, H.W. Kim, Curr. Appl. Phys. 10 (2010) 1017–1021.
[7] S.V. Pol, V.G. Pol, J.M. Calderon-Moreno, S. Cheylan, A. Gedanken, Langmuir 24 (2008) 10462–10466.
[8] L.Y. Chen, D.L. Zhang, G.M. Zhai, J.B. Zhang, Mater. Chem. Phys. 120 (2010) 456–460.
[9] L.D. Yao, F.F. Wang, X. Shen, S.J. You, L.X. Yang, Y.C. Li, K. Zhu, Y.L. Liu, A.L. Pan, B.S. Zou, J. Liu, C.Q. Jin, R.C. Yu, J. Alloys Compd. 480 (2009) 708–801.
[10] B.B. Wang, X.Z. Xu, J. Cryst. Growth 311 (2009) 4759–4762.
[11] D.R.T. Zahn, Appl. Surf. Sci. 123/124 (1998) 276–282.
[12] K. Nagata, T. Ishikawa, Y. Miyamoto, Jpn. J. Appl. Phys. 24 (1985) 1171–1173.
[13] S.L. Zhang, C.L. Yang, Y.T. Hou, Y. Jin, Z.L. Peng, J. Li, S.X. Yuan, Phys. Rev. B52 (1995) 1477–1480.
[14] D. Nesheva, M.J. Ščepanović, S. Aškrabić, Z. Levi, I. Bineva, Z.V. Popović, Acta Phys. Pol. A 116 (2009) 75–77.
[15] J. Wang, W.H. Yao, J.B. Wang, H.Q. Liu, H.H. Sun, X. Wang, Z.L. Pang, Appl. Phys. Lett. 62 (1993) 2845–2847.
[16] T.P. Martin, L. Genzel, Phys. Rev. B8 (1973) 1630–1635.
[17] G. Gouadec, P. Colomban, Progr. Crystal Growth Charact. Mater. 53 (2007) 1–56.